

Study of Phase Wetting in Three-Phase Oil-Water-Gas Horizontal Pipe Flow - Recommendations for Corrosion Risk Assessment

L.D. Paolinelli
Institute for Corrosion and Multiphase Technology
Department of Chemical and Biomolecular Engineering, Ohio University
342 West State Street
Athens, OH 45701
USA

ABSTRACT

Accurate prediction of the phase wetting regime of internal pipe walls of oil production lines is of paramount importance when performing internal corrosion assessments. Therefore, corrosion control costs can be reduced as mitigation efforts can be directly aimed at the most critical pipeline areas where water is most likely to segregate and wet the pipe wall. Surface wetting regime (e.g., oil wet or water wet) depends on several factors, such as flow rates and physicochemical properties of the transported fluids, pipe diameter and inclination, and also pipe surface wettability. This work studies phase wetting regimes in three-phase oil-water-gas horizontal flow in a 0.1 m diameter carbon steel pipe in a flow loop, for flow conditions where liquid-gas slug flow pattern is predominant. Phase wetting and water layer thickness (when water wet) were measured using high frequency impedance probes flush-mounted at the internal pipe wall. Different mechanisms of water wetting are inferred from the obtained data for the bottom and top pipe walls. Maps of phase wetting regime and water layer thickness versus operating conditions are shown for different water cuts. Experimental data is discussed and compared with predictions from a proposed three-phase hydrodynamic model. Consequently, recommendations are provided for direct internal corrosion assessment.

Key words: oil-water-gas flow; phase wetting; water drop-out; modeling; direct internal corrosion assessment

INTRODUCTION

Internal corrosion of production lines is a serious concern in the oil industry. The water phase co-produced with crude oil can be extremely corrosive to carbon steel due to dissolved gases such as CO₂ and H₂S.^{1, 2} When this water is in contact with the metallic pipe wall, in a scenario called water wetting, this can lead to internal corrosion as well as induce other problems such as environmentally assisted cracking and hydrate deposition on the pipe wall.³

If produced water is fully dispersed in oil as continuous phase, water wetting is most likely avoided and corrosion occurrence is insignificant.⁴ Since produced oils are generally less dense than produced water, the water tends to segregate and occupy the pipe bottom in horizontal and slightly inclined lines. Full dispersion or entrainment of water into oil is only possible if the turbulent velocity fluctuations in the

oil flow are sufficient to disrupt the water phase into droplets, keeping them suspended against gravity and preventing their agglomeration and coalescence.

The aforementioned concepts have been theoretically treated for two-phase oil-water pipe flow elsewhere.⁵⁻⁸ For instance, repeated contact of unsuspected water droplets with a hydrophilic pipe wall (e.g., usually carbon steel) can lead to droplet deposition and the formation of water layers and water wetting. On the other hand, excessive accumulation of water droplets (e.g., at the pipe bottom) can lead to droplet agglomeration and coalescence, also developing segregated water layers and water wetting.

Stratified and intermittent/slug gas-liquid flow patterns are common in oil production lines. In these cases, when the volume fraction of produced water relative to the total liquid volume (water cut) is below about 20-30 % (oil dominated liquid), it is of high interest for corrosion engineers to determine if water will be transported fully entrained into the oil or if it will drop out and segregate, wetting the pipe wall. Proper knowledge of phase wetting regime of the internal pipe walls can significantly reduce corrosion control costs as mitigation efforts can directly aim at the most critical pipeline areas where water wetting is likely to occur.

Few studies report liquid flow patterns in three-phase horizontal oil dominated flow. Acikgoz et al.⁹, using a 0.02 m ID flow loop and mineral oil of viscosity 0.116 Pa.s and air, found water-in-oil dispersion in plug and slug flow, and stratified/wavy flow patterns for water cuts as high as 50 % for some specific ranges of gas and liquid superficial velocities. Pan,¹⁰ using a 0.078 m ID flow loop and mineral oil of viscosity 0.04 Pa.s and air at 6 bar ($\times 10^5$ N/m²) pressure, found water-in-oil dispersion in slug flow pattern for liquid superficial velocity of 0.5 m/s and water cuts smaller than about 40 %.

Keskin et al.¹¹ and Ersoy et al.,^{12, 13} using a flow loop of 0.051 m ID and mineral oil of viscosity about 0.02 Pa.s and air, found water-in-oil dispersion for water cuts of 20 % and 40 % for slug and stratified flow with relatively large gas and liquid superficial velocities. They observed that larger values of superficial gas and liquid velocities were needed to disperse water into oil when the water cut was increased. Er et al.,¹⁴ using a similar flow system, studied specifically the onset where the water flow separated from the oil in three-phase stratified flow. They tested different water cuts ranging from 5 % to 40 % with different superficial gas and liquid velocities, and found that increasing superficial gas velocity promoted water-in-oil dispersion.

It is worth mentioning that the characterization of liquid-liquid flow patterns made by Acikgoz et al.,⁹ Pan,¹⁰ Keskin et al.,¹¹ Ersoy et al.,^{12, 13} and Er et al.,¹⁴ were based only on the observation of the flow at clear sections. This could have been imprecise at the time of characterizing, for example, if thin water layers were actually flowing at the pipe bottom. Moreover, plastic or stainless steel pipe walls are mostly hydrophobic, which can also alter the development of segregated water streams compared to hydrophilic pipe walls, as is commonly the case of carbon steel. In this respect, Kee et al.¹⁵ studied flow patterns and phase wetting in horizontal and vertical three-phase flow, using a 0.1 m ID carbon steel pipe section in a flow loop and mineral oil of viscosity of 0.0027 Pa.s and CO₂ as gas phase. The carbon steel test section was equipped with mini flush-mounted DC conductance probes arranged around the pipe circumference to sense the presence of water in contact with the pipe surface. It was found that in horizontal flow with water cut of 1 %, water dropped out at the pipe bottom for superficial gas velocities below about 2 m/s, leading to water wetting. At higher superficial gas velocities, water was mostly dispersed, reducing the extent of water wetting. For higher water cuts of 18 %-20 %, the water wetting behavior prevailed at the lower half of the pipe, and increasing superficial gas velocity did not reduce the extent of water wetting.

The DC conductance probes used in the work conducted by Kee et al., which are sensitive for detection of separated water, represent an improvement with respect to the visual inspection of flow patterns made by other authors in three-phase flow. However, the data generated by Kee et al. is somewhat ambiguous and difficult to use at the time of developing and validating mechanistic models to predict corrosion risk due to water segregation. This is due to the fact that no information of the thickness of the detected water layers was provided. For example, sporadic contact and deposition of dispersed water droplets onto the top pipe wall can be usual in three-phase flow when liquid slugs rapidly wet the entire pipe circumference. This type of water wetting may not develop significant and continuous water

layers that pose as significant a corrosion risk as when water drops out at the pipe bottom due to gravity. In this respect, the use of flush-mounted high frequency (HF) impedance probes can provide not only the phase wetting regime but also the thickness of developed water layers, as shown elsewhere.¹⁶

In regards to the modeling of liquid-liquid flow patterns (e.g., dispersed or separated) in three-phase horizontal pipe flow, limited work has been reported. This is not surprising, given the high complexity of three-phase flow and the limited amount of available experimental data concerning local liquid-liquid flow patterns. Bonizzi et al.¹⁷ proposed a model for slug flow where the size of liquid droplets dispersed in another liquid are calculated using local flow characteristics (e.g., turbulence at the liquid film, or at the slug cylinder) in order to estimate if local liquid-liquid dispersions are stable based on the criteria provided by Brauner.⁵ This model is able to discriminate between stratified and dispersed liquid-liquid flows. However, in this respect, it has not been validated with experimental data. More recently, Er et al.¹⁴ proposed a model to determine onset of water dispersion into oil in three-phase stratified flow based on the occurrence of waves at the oil-water interface that, for relatively low water cuts, reach the pipe bottom and sweep the water phase generating dispersion. This model computes a critical Froude number calculated based on the height of the water layer existing in a stratified gas-oil-water concurrent flow; and therefore, it is unsuitable for slug flow. It is clear that more effort is needed to characterize and predict liquid-liquid dispersion in three-phase slug flow.

The aim of this work is to study phase wetting regimes (e.g., oil wet or water wet) in three-phase oil-water-gas horizontal flow in a large scale flow loop of 0.1 m ID with a carbon steel test section in flow conditions where a slug flow pattern is predominant. Phase wetting regime and water layer thickness (when water wet) were measured using HF impedance probes flush mounted at the internal pipe wall.

Different mechanisms of water wetting are inferred from the obtained data for the bottom and top pipe walls. Maps of phase wetting regime and water layer thickness versus operating conditions (superficial liquid velocity and superficial gas velocity) are shown for different water cuts. A three-phase hydrodynamic model to predict water drop-out in slug flow is introduced and compared with the experimental data. Consequently, recommendations are provided for internal corrosion direct assessment.

EXPERIMENTAL

Large scale flow loop

The flow loop is constructed from 0.1 m ID pipe and consists of two main legs of 15 m length connected with two bends of 90 degrees, as seen in the schematic in Figure 1. The main line (upstream leg) is used for the phase wetting tests and is equipped with a carbon steel test section with impedance probes and a transparent section for flow visualization, both located close to the end of the leg. The main legs of the flow loop are mounted on a steel structure that allows inclination from 0 degrees (horizontal) to 90 degrees (vertical) positions.

The oil flow is fed directly into the main line while the water is directed from the water storage tank through a 0.05 m ID PVC pipe and connected to the main line via a tee-section. The gas stream is introduced into the main line via a 0.1 m ID 45-degree elbow. The mixing of the fluid streams (oil, water and gas) starts at the beginning of the main upstream line of the flow loop (as seen in Figure 1) and develops further downstream through a stainless steel pipe until reaching the phase wetting test section, located at about 140 pipe diameters from the water and gas injection point. The two legs of the flow loop are connected with the rest of the system through a 0.1 m ID and 3 m long flexible hose, which allows for rig inclination.

The liquids were pumped into the main flow line by positive displacement pumps with variable speed electric motors. Liquid flow rates were monitored by turbine and paddle wheel flow meters, connected to a computer for data acquisition and recording. The gas stream was circulated to the main line by a positive displacement lobe-type blower. The gas velocity was measured using hot wire anemometry.

Upon exiting the main line, the flow stream is directed to the separation unit; which includes a gas-liquid separator with droplet separator and an oil-water separator. The separated oil and water streams are returned to their respective storage tanks, made of stainless steel with a capacity of 1.2 m³ each, while dry gas is recirculated by the blower.

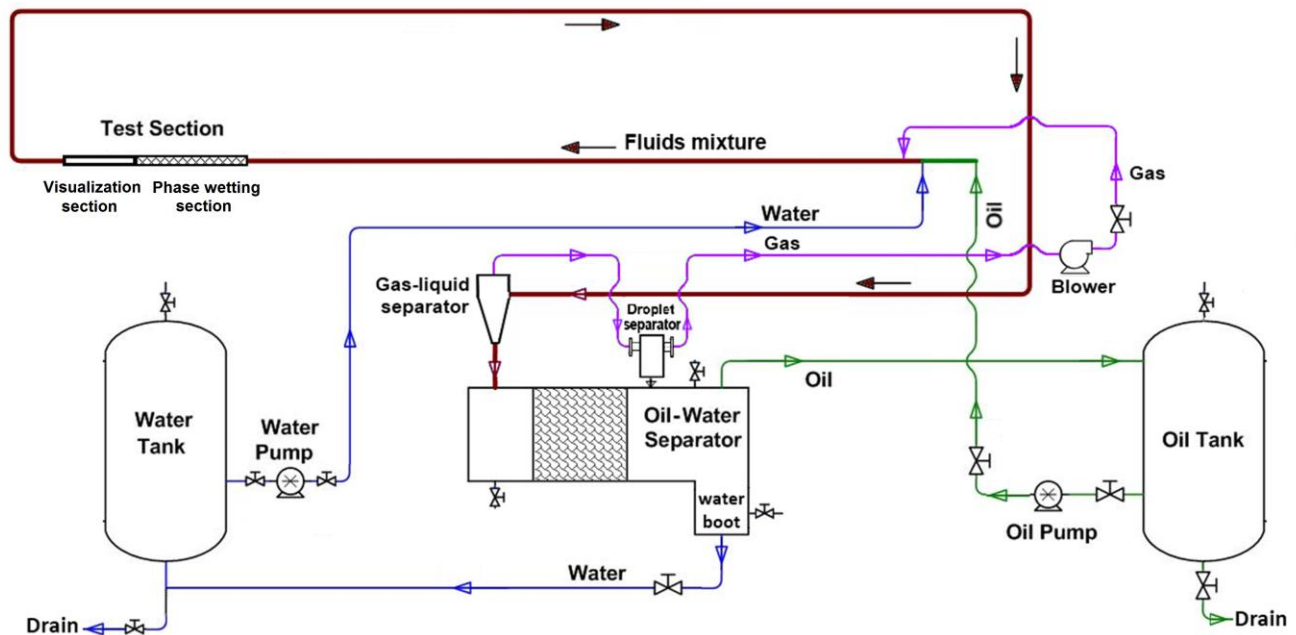


Figure 1: Schematic layout of the 0.1 m ID flow loop used for three phase oil-water-gas flow.

Test section and instrumentation

Phase wetting tests were carried out in a 0.1 m ID and 1.8 m long carbon steel pipe section (Figure 2). Phase wetting regime and thickness of developed water layers were measured using concentric two-electrode high frequency impedance probes, as shown in Figure 3. A single large probe with an inner carbon steel electrode of 12.5 mm diameter ($2r_i$) and an outer stainless steel electrode of 25 mm diameter ($2r_o$) was used flush-mounted at the pipe bottom, where water is most likely to segregate. This configuration was already used to measure phase wetting and water layer thickness in two-phase oil-water flow.¹⁶ Besides, an array of 16 flushed mounted probes of smaller dimensions with two concentric stainless steel electrodes of 3 mm ($2r_i$) and 9.5 mm ($2r_o$) staggered around the pipe circumference was used to detect the presence of water at the top and side pipe walls.

All the probes were operated separately with an AC voltage of 10 mV rms and a frequency of 20 kHz using a Gamry REF 600[†] potentiostat with a computer interface. Once the desired flow conditions were stabilized, the probe wiring was connected to the potentiostat and the impedance measurements were performed continuously for at least 2 min using a sampling period of approximately 0.5 seconds. The presence of water layers in contact with the probe, and their thickness, was determined from the measured impedance values (modulus and phase angle) in relation to the theoretical response of the probe and the electrical conductivity of the water phase, as reported elsewhere.¹⁶

Before each set of experimental runs, where about 6 flow conditions were tested, the internal surface of the test section was polished using a rotating flexible abrasive tool (180 grit) with deionized water as

[†] Trade name

the polishing fluid. The surface was then washed with deionized water and isopropanol, then dried with a clean cloth.

Static wetting experiments of water-in-oil contact angles were also performed, using a goniometer, on the surface of a carbon steel specimen, prepared using the same procedure as for the test section. It was determined that the carbon steel surface exhibits hydrophilicity after some seconds, giving water-in-oil contact angles of about 60° (measured from the inside of the sessile water droplet).

A clear acrylic section was located just downstream of the carbon steel test section to allow visualization of the developed flow patterns, recorded as pictures and videos using a high-resolution digital camera. When slug flow was present, the average frequency between liquid slugs was measured from the recorded videos.

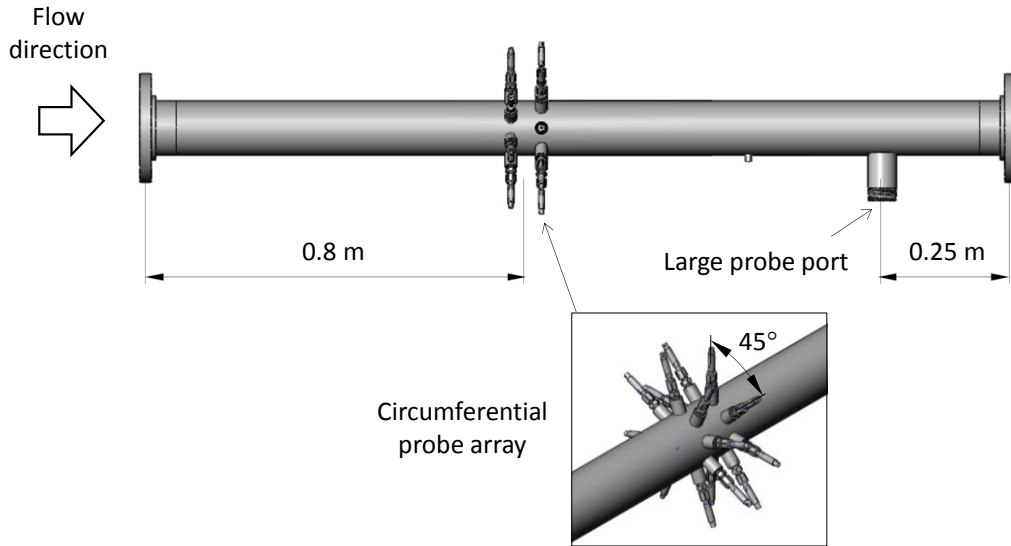


Figure 2: Schematic of the carbon steel test section used for phase wetting measurements.

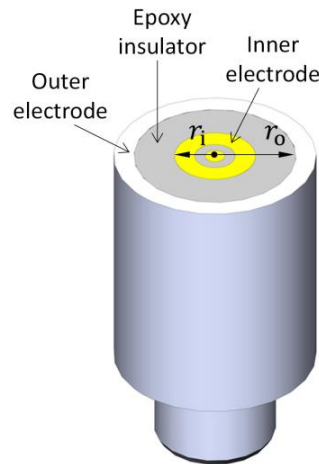


Figure 3: Schematic of the concentric two-electrode impedance probe.

Test fluids

Isopar V[†], a clear saturated paraffinic hydrocarbon, was used as the oil phase. The water phase was 1 wt.% NaCl solution prepared from deionized water. Air was used as the gas phase. The properties of the test fluids are listed in Table 1.

The use of a highly conductive electrolyte as water phase (1.76 S/m) helps preventing significant local conductivity changes when the solution comes in contact with the carbon steel test section, which may corrode and release iron ions.

The oil-water inversion point is indicated as water phase volumetric concentration. It was measured in a stirred vessel using two-electrode HF impedance measurements.

Table 1: List of properties of the test fluids (values at 25 °C).

Property	Oil	Water	Gas
Density (kg/m ³)	810	1005	1.12
Dynamic viscosity (Pa.s)	0.01	0.001	17 _x 10 ⁻⁶
Surface tension (N/m)	0.03	0.072	-----
Oil-water interfacial tension (N/m)	0.049		N/A
Oil-water inversion point (%)	25		N/A

Test flow conditions

Flow experiments were performed in horizontal condition at room temperature (~25 °C) and atmospheric pressure using different superficial liquid velocities, superficial gas velocities and water cuts. Table 2 lists the conditions used in the flow tests.

Table 2: Conditions used in the flow tests.

Parameter	Value
Superficial liquid (oil+water) velocity (m/s)	0.1 – 1.5
Superficial gas velocity (m/s)	1 – 20
Water cut (%)	1 – 10

The maximum uncertainty in the oil superficial velocity and the water superficial velocity values was 10 % and 15 %, respectively. The maximum uncertainty in the superficial gas velocity was 15 %, for values lower than 10 m/s, and 20 % for larger velocities.

Each flow condition was repeated at least twice, showing good reproducibility. The experimental data shown in the results section are the average of at least two independent runs. Once a flow condition was set, it was run for about 10 minutes before measuring phase wetting regime and recording flow pattern.

[†] Trade name

RESULTS

Characterization of gas-liquid flow patterns

Figure 4 shows the gas-liquid flow patterns observed for the different used superficial liquid and gas velocities and water cuts. Slug flow is predominantly found in the range of superficial liquid velocities (u_{sl}) from 0.3 m/s to 1.5 m/s and superficial liquid velocities (u_{sg}) from 1 m/s to 10 m/s, which is somewhat in line with the stratified to non-stratified transition estimated with the Taitel and Dukler model (solid line).¹⁸ A transition to an annular wavy flow pattern is seen at u_{sg} values of 20 m/s and u_{sl} values lower than 1 m/s, or u_{sg} values of 10 m/s and u_{sl} values lower than 0.5 m/s, in agreement with the criterion suggested by Barnea of liquid holdup (α_1) larger or equal to 0.24 for intermittent flow (dash-dot line).¹⁹ Elongated bubble and stratified flow patterns are found for a superficial liquid velocity of 0.1 m/s. Increasing the water cut from 1 % to 10 % does not alter gas-liquid flow patterns. Similar behavior has been reported elsewhere.¹⁵ Figure 5 shows examples of slug flow patterns observed from the side of the pipe clear section located downstream of the carbon steel test section for $u_{sg} = 1$ m/s and 1 % water cut and u_{sl} values of 0.5 m/s and 1.5 m/s. It can be seen that for the lower superficial liquid velocity (0.5 m/s), water is distributed mostly at the pipe bottom semi-dispersed as water globules. For the larger superficial liquid velocity (1.5 m/s), the water phase is distributed more uniformly in the liquid mixture.

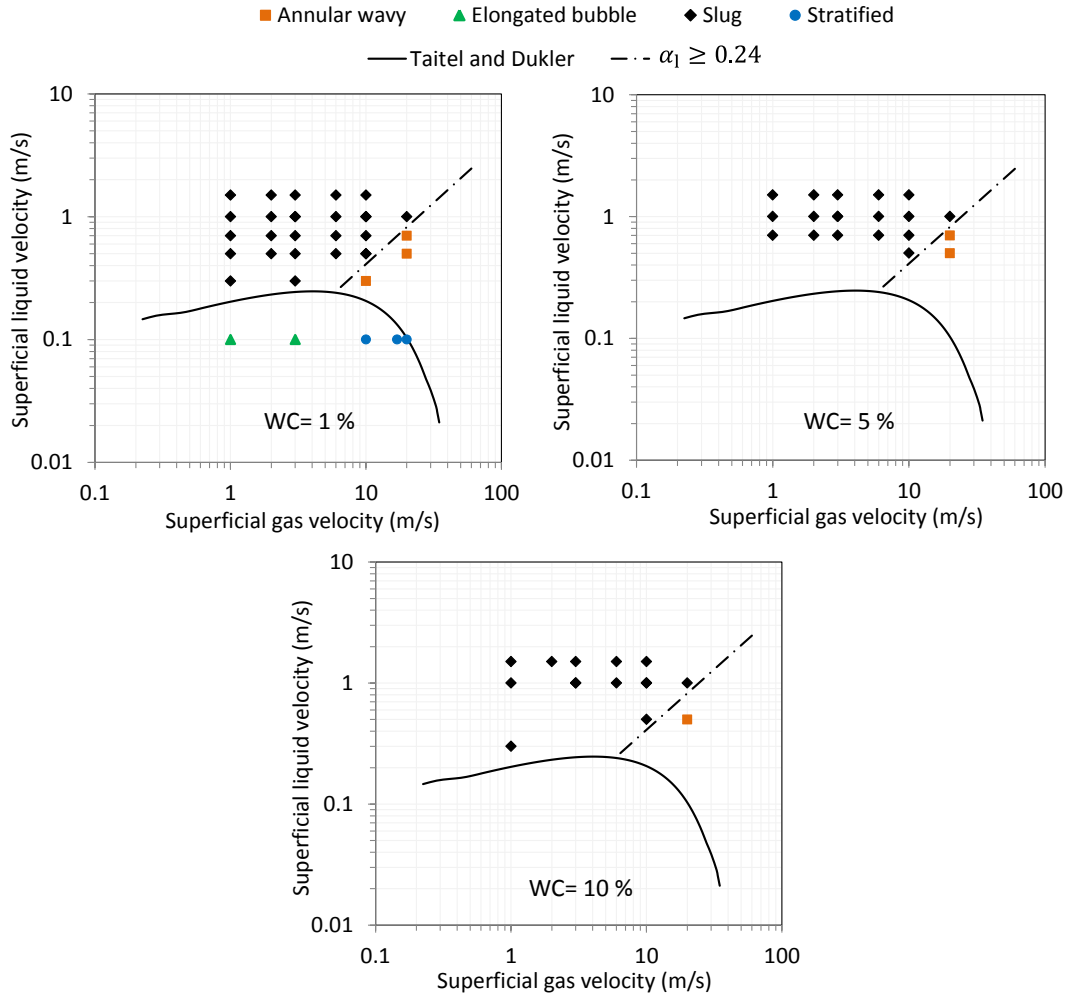


Figure 4: Gas-liquid flow patterns found for horizontal oil-water-gas flow with different water cuts.

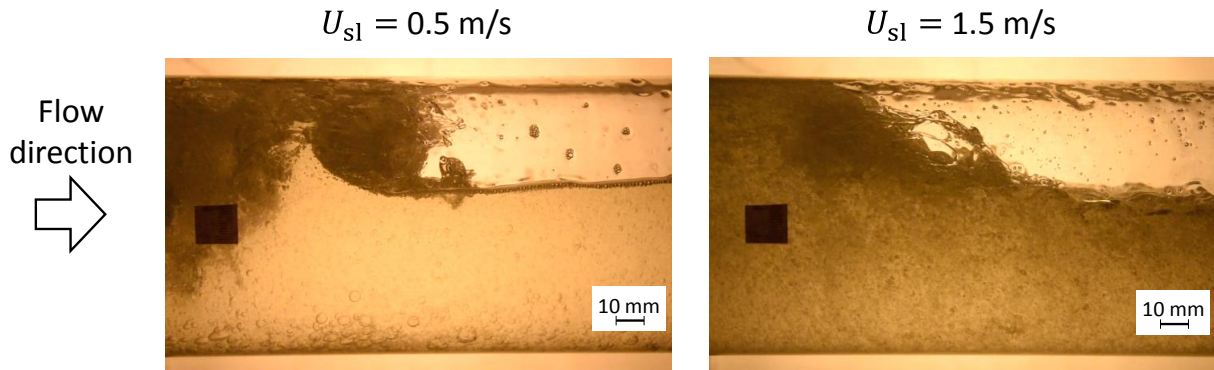


Figure 5: Example of slug flow patterns observed from the side of a clear section in horizontal oil-water-gas flow. Superficial gas velocity (u_{sg}) of 1 m/s and 1 % water cut.

Characterization of phase wetting and water layer thickness

Water layers developed around the pipe circumference

Figures 6 and 7 show examples of time-averaged water layer thickness estimated from HF impedance measurements on some of the small probes located around the pipe test section in three-phase slug flow with 5 % and 10 % water cut, respectively. Error bars show maximum and minimum values. It is worth mentioning that the lowest water layer thickness that can be detected by the used setup is about 0.003 mm on average. No evidence of water or corrosion was found for impedance measurements equivalent to water layer thicknesses lower than this value as found elsewhere;¹⁶ therefore, estimated thicknesses below 0.003 mm (dashed line) are considered as oil wet (positions marked with black triangles). It can be seen that for relatively low gas superficial velocity ($u_{s1} = 1$ m/s), water drops out from dispersion due to gravity forming water layers that have maximum thickness at the pipe bottom (6 o'clock position). For example, average thicknesses of ~0.3 mm and ~0.7 mm are measured for 5 % and 10 % water cut, respectively. It is worth noting that thin water films from 0.01 mm to 0.1 mm thickness are also detected at the upper half of the pipe. The occurrence and thickness of these thin films are irregular along the upper pipe perimeter.

Increasing superficial gas velocity (for example, 6 m/s and 10 m/s for 5 % and 10 % water cut, respectively), water droplets can be effectively entrained by the oil flow as no water layer is detected at the pipe bottom. However, thin water films with average thickness smaller than 0.1 mm still form at the upper half of the pipe, especially for the largest water cut of 10 %.

The thickness of the water layer developed at the pipe walls can vary significantly with time as inferred from the error bars in Figures 6 and 7. This is mainly related to the intermittent nature of slug flow. Figure 8 shows a clear example where the pattern of variation in time of the water layer thickness measured at the pipe bottom coincides with the average measured time between slugs, which is about 6 seconds for this flow condition. Water preferentially segregates at the liquid film region and then is partially or totally swept off and entrained by the passage of the liquid slugs. These effects can lead to either intermittent water wet or intermittent oil wet regimes.

Figure 9 shows an example of water layer thickness as a function of time measured at different locations of the pipe circumference. Similarly, as also seen in Figure 8, the variation of the water layer thickness monitored at the pipe bottom somewhat correlates with the average measured time between slugs (~3.5 seconds). On the other hand, it is difficult to infer if the water layer thickness monitored at the top and side of the pipe vary in accordance with the average period between slugs. The formation of water films at the upper half of the pipe would be related to the sporadic deposition of dispersed water droplets that rapidly come in contact with the pipe wall when slugs are developed. In this case, droplet deposition may not always happen when each slug passes, since it depends on variable factors such as the size, velocity and impact angle of the impinging water droplets. The combination of these

factors can produce quite different effects when water droplets impact the top and side pipe walls, such as due to deposition or rebound.²⁰ Moreover, oil films are commonly found attached to the upper pipe surface between slugs (as seen in Figure 5), and drip by gravity from the top to the side pipe walls. These films can alter the wettability of the pipe surface (e.g., turning it hydrophobic) as well as damp the impact of contacting water droplets (“cushioning”); both effects tend to reduce droplet deposition. The thickness of the thin water films monitored at the upper half of the pipe tends to increase with water cut. This is in line with the fact that more water droplets per unit of volume of liquid mixture are available to be deposited onto the pipe surface.

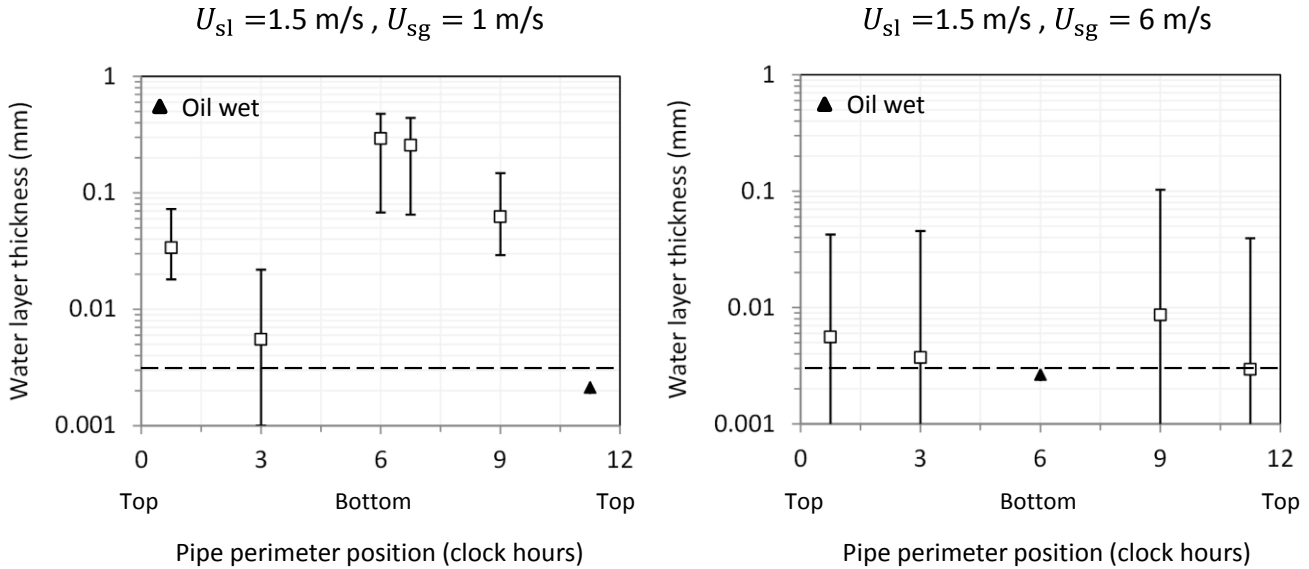


Figure 6: Example of time-averaged water layer thickness estimated from HF impedance measurements around the pipe circumference in three-phase horizontal slug flow with 5 % water cut and different superficial gas velocities.

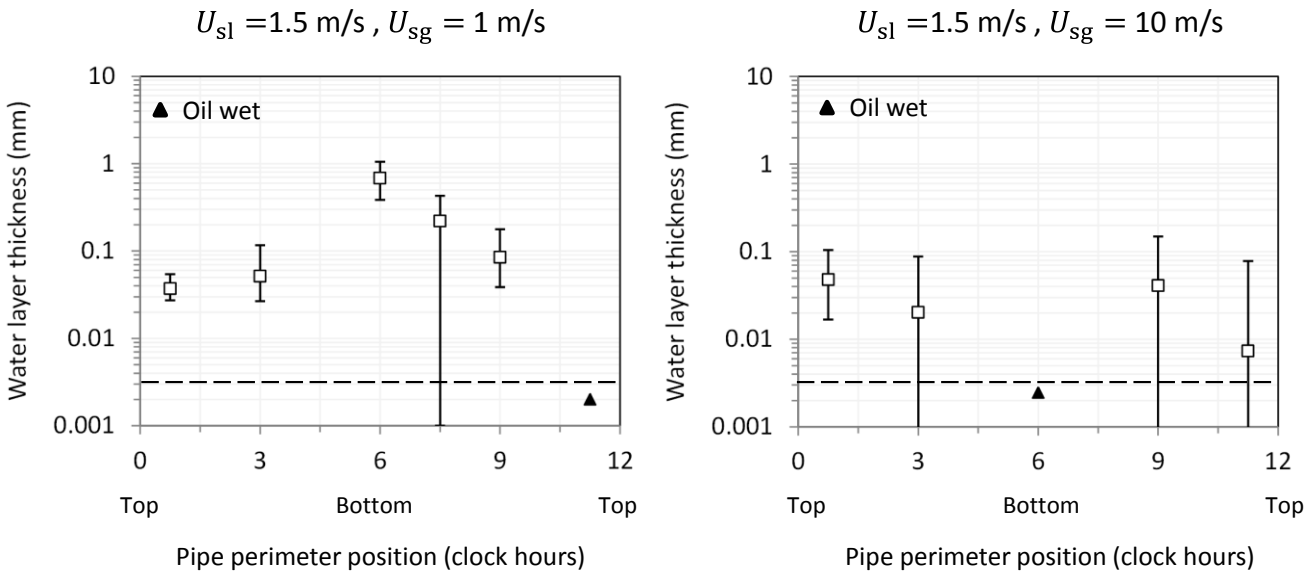


Figure 7: Example of time-averaged water layer thickness estimated from HF impedance measurements around the pipe circumference in three-phase horizontal slug flow with 10 % water cut and different superficial gas velocities

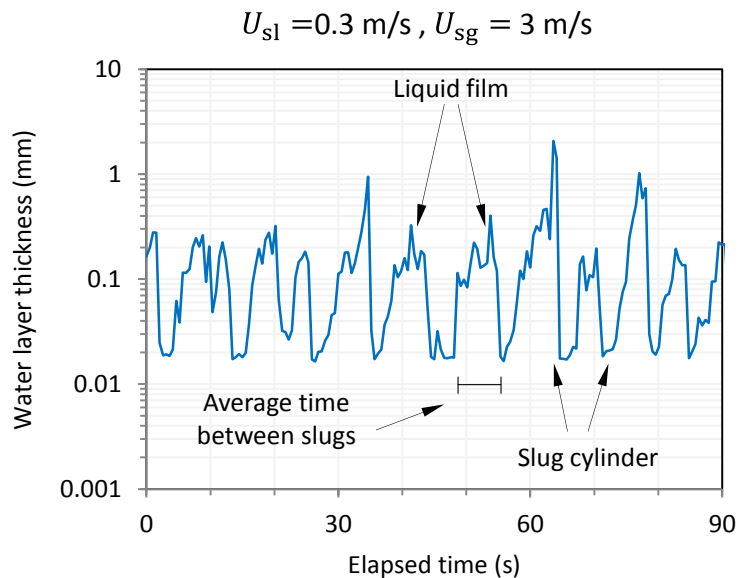


Figure 8: Example of water layer thickness measured at the pipe bottom in function of time in three-phase horizontal slug flow with 1 % water cut.

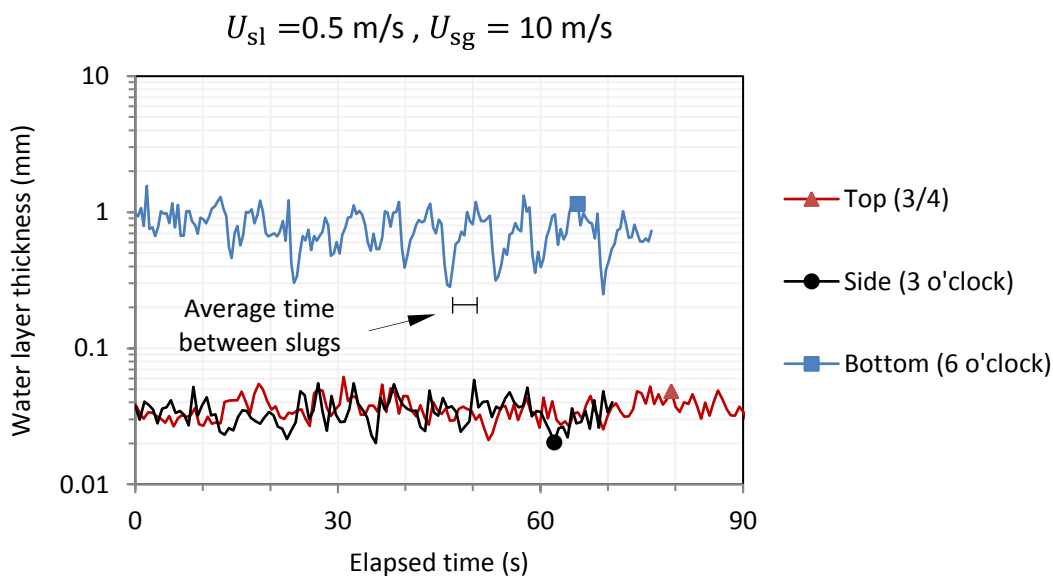


Figure 9: Example of water layer thickness measured at the pipe circumference in function of time in three-phase horizontal slug flow with 10 % water cut.

In general, two types of water wetting scenarios are found in three-phase slug flow in carbon steel pipe. The first is the formation of water layers at the pipe bottom due to gravity; for example, by deposition and agglomeration and coalescence of sinking water droplets at the pipe bottom. The second is the sporadic deposition of water droplets at the upper half of the pipe due to rapid contact of the liquid mixture with the pipe surface when slugs are formed.

The latter may not be considered as a serious problem since, in general, natural components of crude oil (e.g., organic acids) can alter carbon steel surface making it hydrophobic.^{21, 22} In this context, droplets would not easily deposit at the upper pipe wall preventing the formation of water films. Moreover, if very thin water films (smaller than 0.1 mm thickness) are formed, they might be rapidly

saturated with, e.g., ferrous ions from the occurring corrosion processes due to their large surface/volume ratio and limited replenishment promoting the formation of protective corrosion product layers. On the other hand, water drop-out due to gravity is the most serious concern since water accumulates predominantly at the pipe bottom.

Phase wetting regimes and water layer thickness at the pipe bottom

All the surface wetting and water layer thickness maps reported in this section are based on the information obtained using the single large HF impedance probe located at the pipe bottom (see Experimental section). This larger probe senses a wider area than the smaller probes; thus, it is considered more adequate for characterizing the average phase wetting behavior at the bottom of the pipe.

As described above, the water streams detected in contact with the bottom pipe wall showed intermittent variation of their thickness with time. Moreover, in some cases the occurrence of free water at the pipe wall was alternating. This led to a wide categorization of the measured phase wetting regimes, which are described as follows:

- Full oil wet: water is not detected or it is detected less than 30 % of the measuring time with layer thickness lower than 0.1 mm.
- Transitional: water is detected more than 30 % of the time but only with a layer thickness lower than 0.1 mm.
- Unstable oil wet: water is detected less than 30 % of the time with layer thickness larger than 0.1 mm.
- Unstable water wet: water is detected between 30 % and 70 % of the time with layer thickness larger than 0.1 mm.
- Water wet: water is detected more than 70 % of the time with layer thickness larger than 0.1 mm.

Figures 10, 11 and 12 show the measured phase wetting regimes for 1 %, 5 % and 10 % water cut, respectively. In the case for water wet, unstable water wet and unstable oil wet regimes, the estimated time-averaged water layer thickness is also appraised in ranges to illustrate their variation with flow conditions (e.g., hollow green triangles indicate average water layer thicknesses between 0.1 mm and 0.5 mm).

An oil wet regime can be achieved by increasing both superficial liquid and gas velocities. Superficial liquid velocity plays a more important role since a relatively small variation of this parameter is needed to fully disperse transported water when compared to the effect of superficial gas velocity, as seen from the slope of the experimental oil wet to water wet transition indicated as dashed lines in Figures 10, 11 and 12. Either unstable water wet or unstable oil wet is seen close to the phase wetting transition boundary. This is unsurprising since intermittent formation and entrainment of water layers is expected in slug flow, as discussed above. Detected water layers are relatively thin on average (e.g., between 0.1 mm and 0.5 mm) for these flow conditions, and become thicker for lower superficial liquid and gas velocities where water drop-out is favored.

Larger superficial liquid and gas velocities are required to fully disperse the water phase when water cut increases. This is in line with other research on phase wetting²³ and flow patterns.¹¹⁻¹³ It is noteworthy that water wetting can be avoided at superficial liquid velocities as low as 0.5 m/s for 1 % water cut, provided that superficial gas velocity is larger than 3 m/s. On the other hand, superficial liquid velocities as high as 1.5 m/s and superficial gas velocities of 2 m/s or more are needed to avoid water segregation at the pipe bottom for water cuts of 5 % and 10 %.

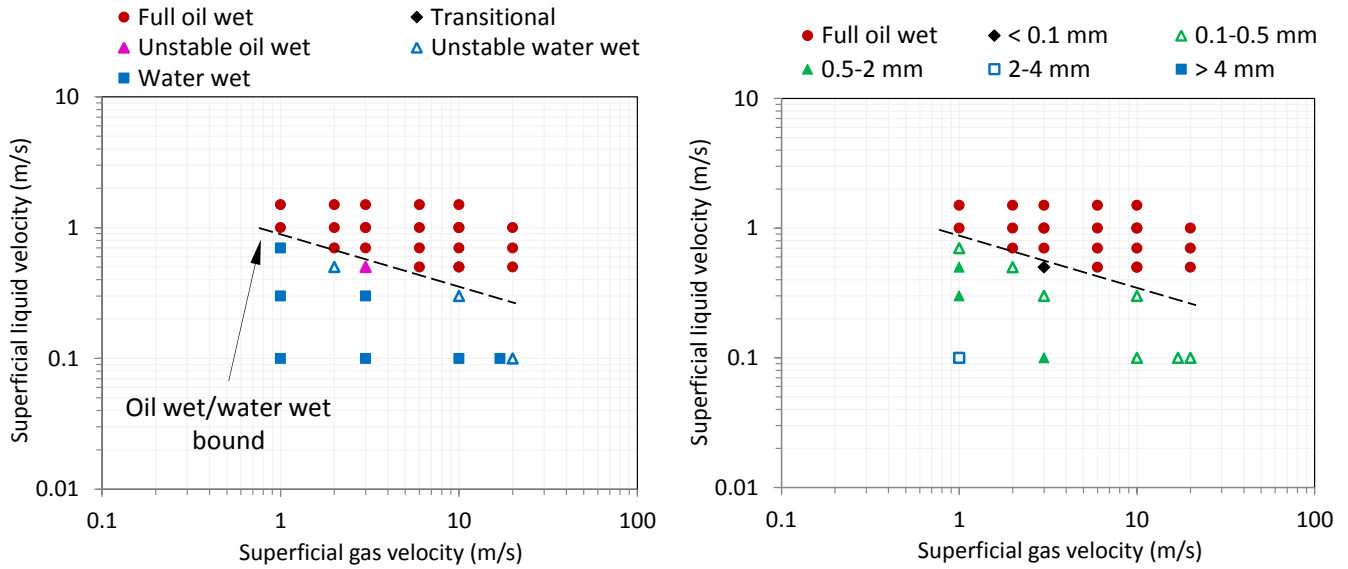


Figure 10: Phase wetting regime (left) and time-averaged water layer thickness (right) measured at the bottom of a carbon steel pipe for different superficial gas and liquid velocities in three-phase horizontal slug flow with 1 % water cut.

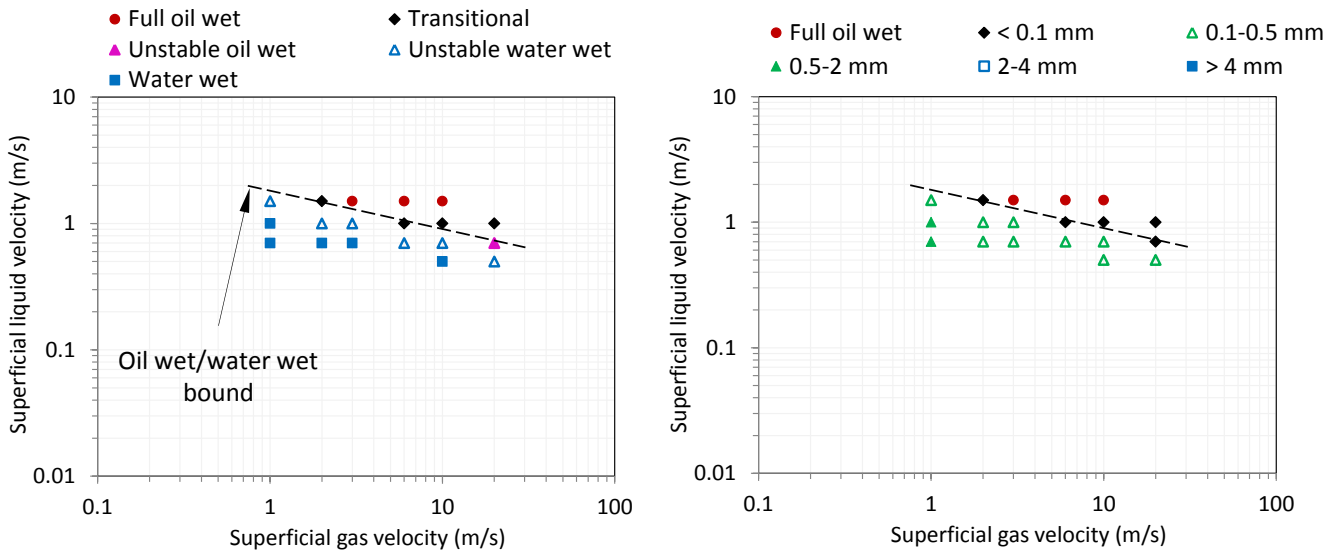


Figure 11: Phase wetting regime (left) and time-averaged water layer thickness (right) measured at the bottom of a carbon steel pipe for different superficial gas and liquid velocities in three-phase horizontal slug flow with 5 % water cut.

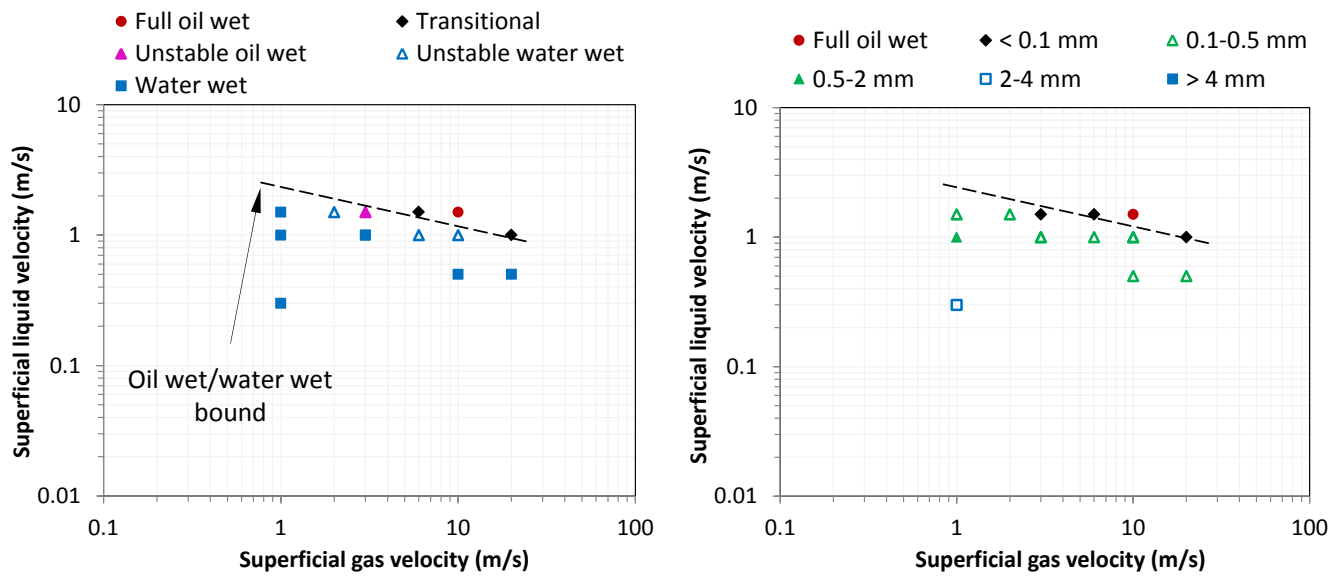


Figure 12: Phase wetting regime (left) and time-averaged water layer thickness (right) measured at the bottom of a carbon steel pipe for different superficial gas and liquid velocities in three-phase horizontal slug flow with 10 % water cut.

On modeling of liquid-liquid dispersion onset in three-phase slug flow

Water drop-out and water wetting can be avoided if full dispersion of water in oil is achieved in the liquid mixture. To estimate the onset of full liquid-liquid dispersion, available criteria provided by Brauner⁵ and other proposed criteria are adapted for liquid slug flow. It is assumed that the liquid mixture is already dispersed, and stability criteria are evaluated relating to the liquid mixture flow. A simplified steady state liquid-gas slug flow model, where the liquid film region has a constant thickness (see Figure 13), is used to estimate the liquid mixture flow characteristics at the film and slug cylinder regions.

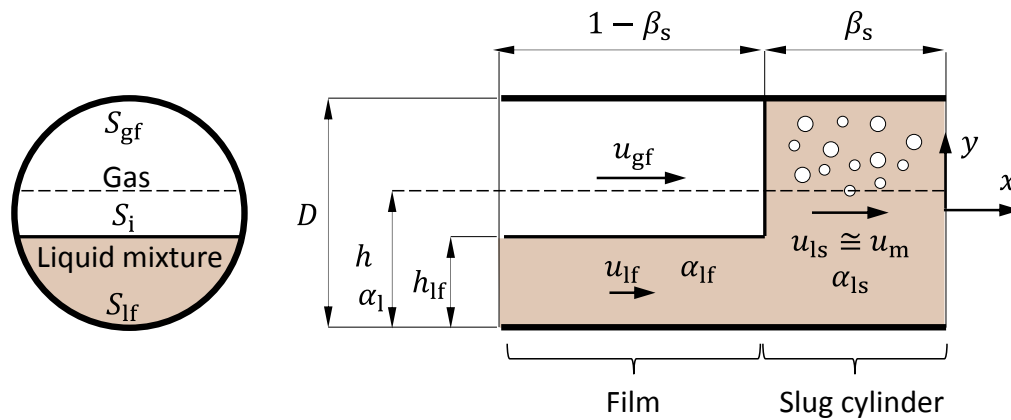


Figure 13: Schematic representation of the slug flow unit assumed in the gas-liquid model.

Gas-liquid slug flow model

The gas bubble/liquid film region of the slug unit can be modeled by using the combined momentum balance at steady state for stratified liquid and gas in a pipe:

$$\frac{\tau_{gf}S_{gf}}{\alpha_{gf}} - \frac{\tau_{lf}S_{lf}}{\alpha_{lf}} + \tau_i S_i \left(\frac{1}{\alpha_{lf}} + \frac{1}{\alpha_{gf}} \right) - A(\rho_l - \rho_g)g \sin \beta = 0 \quad (1)$$

where τ_{gf} (Pa) and τ_{lf} (Pa) are the wall shear stresses due to the flow of the gas bubble and the liquid film, respectively; τ_i (Pa) is the shear stress at the gas-liquid interface, α_{gf} (also expressed as: $1 - \alpha_{lf}$) and α_{lf} are the fractions of pipe cross sectional area (A , m²) occupied by gas and liquid, respectively; S_{gf} (m) and S_{lf} (m) are the pipe perimeters wetted by gas and liquid, respectively; S_i (m) is the perimeter of the gas-liquid interface, ρ_g (kg/m³) and ρ_l (kg/m³) are the densities of gas and liquid, respectively; g (m/s²) is the gravitational acceleration, and β (rad) is the pipe inclination angle measured from the horizontal.

The wall shear stresses are calculated as follows:

$$\tau_{gf} = \frac{1}{2} f_{gf} \rho_g u_{gf}^2 \quad (2)$$

$$\tau_{lf} = \frac{1}{2} f_{lf} \rho_l u_{lf}^2 \quad (3)$$

and the interfacial stress:

$$\tau_i = \frac{1}{2} f_i \rho_g (u_{gf} - u_{lf}) |u_{gf} - u_{lf}| \quad (4)$$

where u_{gf} (m/s) and u_{lf} (m/s) are the mean velocities of the gas and liquid; respectively; and f_{gf} , f_{lf} and f_i are the friction factors for the gas bubble, liquid film and gas-liquid interface, respectively. Friction factors are estimated as:

$$f = C Re^{-n} \quad (5)$$

where Re is the Reynolds number, and C and n are constants equal to 0.046 and 0.2, respectively; for turbulent flow $Re > 2100$, and 16 and 1 for laminar flow $Re \leq 2100$. The Reynolds number for the gas bubble flow:

$$Re_g = \frac{\rho_g u_{gf} D_{gf}}{\mu_g} \quad (6)$$

liquid film flow:

$$Re_{lf} = \frac{\rho_l u_{lf} D_{lf}}{\mu_l} \quad (7)$$

and gas-liquid interface, which is also considered smooth:

$$Re_i = \frac{\rho_g |u_{gf} - u_{lf}| D_{gf}}{\mu_g} \quad (8)$$

where μ_g (Pa.s) and μ_l (Pa.s) are the viscosities of the gas and the liquid, respectively; D_{gf} is the hydraulic diameter for the gas bubble flow:

$$D_{gf} = \frac{4A\alpha_{gf}}{S_{lg} + S_i} \quad (9)$$

and D_{lf} is the hydraulic diameter of the liquid film flow:

$$D_{lf} = \frac{4A\alpha_{lf}}{S_{lf}} \quad (10)$$

The mean velocity of the liquid slug cylinder (u_{ls} , m/s) is approximated to the mixture velocity ($u_{ls} = u_m$), which is calculated as the summation of superficial gas and liquid velocities:

$$u_m = u_{sg} + u_{sl} \quad (11)$$

No slip is considered between the entrained gas bubbles and the liquid in the slug cylinder.

Then velocities of the gas bubble and the liquid film can be related with the gas bubble and liquid film holdups (α_{gf} and α_{lf} , respectively) as proposed by Dukler and Hubbard:²⁴

$$u_{gf} = u_t + (u_m - u_t) \left(\frac{1 - \alpha_{ls}}{1 - \alpha_{lf}} \right) \quad (12)$$

$$u_{lf} = u_t \left(1 - \frac{\alpha_{ls}}{\alpha_{lf}} \right) + u_m \frac{\alpha_{ls}}{\alpha_{lf}} \quad (13)$$

where α_{ls} is the liquid holdup at the slug cylinder, u_t (m/s) is the translational velocity at which the slug propagates, and is estimated as:

$$u_t = C_0 u_m + u_b \quad (14)$$

where u_b (m/s) is the Taylor bubble velocity that can be neglected in horizontal slug flow, C_0 is the distribution parameter used in the drift-flux model and can be approximated with the value 1.2.²⁵

The liquid holdup at the slug cylinder is approximated using the Gregory et al. correlation:²⁶

$$\alpha_{ls} = \left[1 + \left(\frac{u_m}{8.66} \right)^{1.39} \right]^{-1} \quad (15)$$

Note that the constant 8.66 in equation (15) has velocity units.

Finally, the combined momentum balance in equation (1) can be solved iteratively to find the liquid film holdup (α_{lf}). It is worth mentioning that equation (1) has multiple roots for pipe inclination angles (β) different than zero. In general, the smaller root is considered as solution of the problem.

Subsequently, the wall shear stress at the liquid slug (τ_{ls}) is estimated as:

$$\tau_{ls} = \frac{1}{2} f_{ls} \rho_l u_m^2 \quad (16)$$

The friction factor of the liquid slug (f_{ls}) is calculated with equation (5) using the Reynolds number:

$$Re_{lf} = \frac{\rho_l u_m D}{\mu_l} \quad (17)$$

where D (m) is the pipe internal diameter.

From the conservation of the liquid mass in the slug unit (liquid film + slug cylinder), the relative length of the slug cylinder can be estimated in terms of the superficial liquid velocity (u_{sl} , m/s) and the velocities and the liquid holdups of the film and the slug cylinder:

$$\beta_s = \frac{u_{sl} - u_{lf} \alpha_{lf}}{u_m \alpha_{ls} - u_{lf} \alpha_{lf}} \quad (18)$$

Then, the average liquid holdup in the slug unit is:

$$\alpha_l = \alpha_{ls} \beta_s + \alpha_{lf} (1 - \beta_s) \quad (19)$$

The slug frequency (Hz) can be estimated using the correlation introduced by Gregory and Scott:²⁷

$$f_s = 0.0226 \left[\frac{u_{sl}}{gD} \left(\frac{19.75}{u_m} + u_m \right) \right]^{1.2} \quad (20)$$

Note that the constant 19.75 in equation (20) has velocity units. Although equation (20) represents fairly well the experimental results obtained in the used flow loop, accurate slug frequency or absolute slug length calculation requires tracking of the slug front/end by numerical models using the exact details of the pipeline profile and upstream and downstream geometrical constraints.

Liquid-liquid mixture properties

It is assumed that the water phase is well dispersed into the oil and there is no slip between phases. Therefore, the volumetric water content in the liquid mixture (ε_w) is similar to the water cut:

$$\varepsilon_w = \frac{u_{sw}}{u_{sw} + u_{so}} = \frac{u_{sw}}{u_{sl}} \quad (21)$$

where u_{sw} (m/s) is the superficial water velocity and u_{so} (m/s) is the superficial oil velocity. Their summation leads to the superficial liquid velocity (u_{sl}).

Then, the density of the liquid mixture is estimated as:

$$\rho_l = \varepsilon_w \rho_w + (1 - \varepsilon_w) \rho_o \quad (22)$$

where ρ_w (kg/m³) and ρ_o (kg/m³) are the densities of the water and the oil phases, respectively.

The mixture viscosity is considered similar to the viscosity of the continuous phase and is corrected by the volumetric fraction of dispersed phase using the Brinkman equation,²⁸ for example, for oil dominated flow:

$$\mu_l = \mu_o (1 - \varepsilon_w)^{-2.5} \quad (23)$$

where μ_o (Pa.s) is the viscosity of the oil.

Liquid-liquid dispersion criteria

The criteria provided by Brauner⁵ are commonly used to assess the stability of liquid-liquid dispersion in pipes.

It must be assured that droplets of dispersed phase are suspended against gravity by the turbulent flow forces exerted by the continuous phase. In the case of oil dominated flow, this can be expressed as:

$$d_{cb} = \frac{3}{4} \frac{\rho_o}{(\rho_w - \rho_o)g \cos \beta} C_D v'^2 \quad (24)$$

where d_{cb} (m) is the critical droplet size above which droplets will sink and contact the pipe wall, C_D is the droplet drag coefficient that Brauner approximates as 1, but can be better estimated using the Schiller-Naumann correlation:²⁹

$$C_D = \frac{24}{Re_p} (1 + 0.15 Re_p^{0.687}) \quad (25)$$

where Re_p is the droplet Reynolds number:

$$Re_p = \frac{\rho_o v' d}{\mu_o} \quad (26)$$

where d (m) is the droplet size, and v' (m/s) is the mean turbulent velocity fluctuations (rms) of the continuous phase in the radial direction of the pipe, commonly approximated as equal to the friction velocity (u^* , m/s). In the case of slug flow, the latter parameter can be calculated as the average of its values at the liquid film (u^*_{lf}) and the slug cylinder (u^*_{ls}) regions:

$$v' \cong \bar{u}^* = u^*_{ls} \beta_s + u^*_{lf} (1 - \beta_s) = \sqrt{\frac{\tau_{ls}}{\rho_o}} \beta_s + \sqrt{\frac{|\tau_{lf}|}{\rho_o}} (1 - \beta_s) \quad (27)$$

Water droplets must also be smaller than a critical size where they are excessively deformed, and consequently unable to be effectively ejected from the pipe wall:

$$d_{c\sigma} = \left[\frac{0.4\sigma}{(\rho_w - \rho_o)g \cos \beta} \right]^{1/2} \quad (28)$$

where σ (N/m) is the oil-water interfacial tension.

Then, the critical droplet diameter (m) is estimated as:

$$d_{crit} = \text{Min}(d_{cb}, d_{c\sigma}) \quad (29)$$

The combined transitional criterion for dispersed flow is:

$$d_{max} \leq d_{crit} \quad (30)$$

where d_{max} (m) is the maximum water droplet size that can be estimated using the Hinze model³⁰ for diluted dispersions:

$$d_{max,0} = 0.725 \left(\frac{\sigma}{\rho_o} \right)^{3/5} \epsilon^{-2/5} \quad (31)$$

where ϵ (Watt/kg) is the mean energy dissipation rate of the oil flow. The multiplication factor provided by Mlynek and Resnik³¹ is used to correct $d_{\max,0}$ for different volumetric water contents:

$$d_{\max} = d_{\max,0}(1 + 5.4 \epsilon_w) \quad (32)$$

The mean energy dissipation rate of the oil flow can be estimated as the average of its values at the liquid film (ϵ_{lf}) and the slug cylinder (ϵ_{ls}) regions:

$$\epsilon = \epsilon_{ls} \beta_s + \epsilon_{lf} (1 - \beta_s) = \frac{1}{\rho_o} \left[\frac{4 \tau_{ls} u_m}{D \alpha_{ls} (1 - \epsilon_w)} \beta_s + \frac{S_{lf} |\tau_{lf}| |u_{lf}|}{A \alpha_{lf} (1 - \epsilon_w)} (1 - \beta_s) \right] \quad (33)$$

It is also considered that if the predicted maximum droplet size (d_{\max}) is smaller than 3 times the predicted liquid film height (h_{lf} , Figure 13), the water droplets cannot be effectively suspended against gravity. This concept is based on the fact that larger water droplets can only be suspended by eddies of similar or larger length scales, which are required to fit between the droplets and the pipe wall.³² Therefore, for full liquid-liquid dispersion, equation (30) as well as the following relationship must be satisfied:

$$h_{lf} \geq 3d_{\max} \quad (34)$$

Figures 14, 15 and 16 show the dispersed flow transition line calculated with equations (30) and (34) ($d_{\max} \leq d_{\text{crit}}$ and $h_{lf} \geq 3d_{\max}$, solid black line) on the phase wetting and water layer thickness maps of Figures 10, 11 and 12, respectively. It can be seen that the combination of equations (30) and (34) describes fairly well the water wet to oil wet transition for the flow with 1 % water cut (Figure 14), in the region where slug flow is present (left from the dash-dot black line, slug to annular flow transition). However, for 5 % and 10 % water cut, the calculated transition lines underpredict the experimental phase wetting transition by a factor 2 to 3 in terms of superficial liquid velocity.

It is worth mentioning that if the critical droplet size d_{cb} is calculated considering only the turbulent characteristics of the liquid film ($\beta_s=0$), which is the most conservative assumption as discussed by Pots et al.,³³ the transition lines (dot black lines) show a steeper slope and overpredict critical superficial liquid velocity values with respect to the experimental phase wetting transition; especially in the case of 1 % and 5 % water cut (Figures 14 and 15).

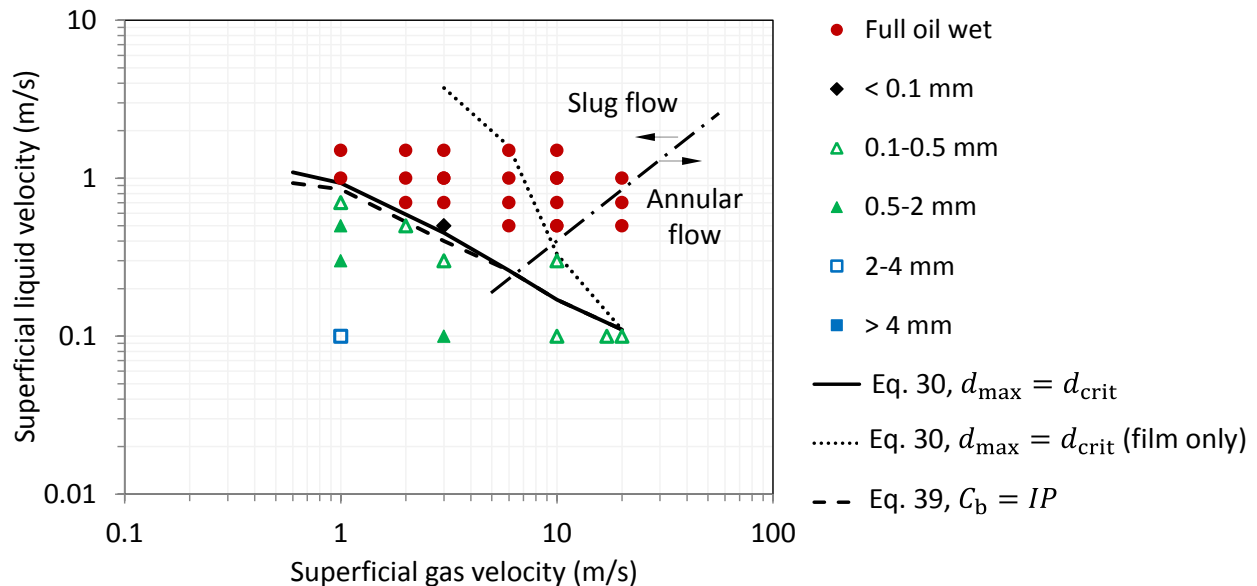


Figure 14: Modeled transition lines for dispersed liquid-liquid flow on experimental maps of phase wetting and water layer thickness at the bottom of a carbon steel pipe for different superficial gas and liquid velocities in three-phase horizontal slug flow with 1 % water cut.

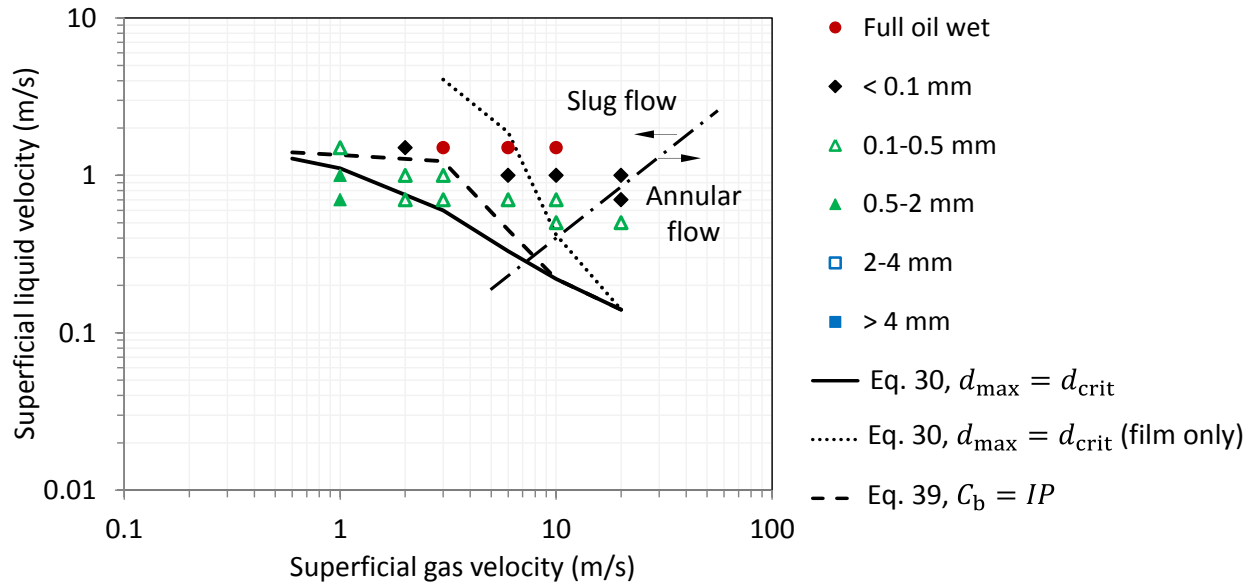


Figure 15: Modeled transition lines for dispersed liquid-liquid flow on experimental maps of phase wetting and water layer thickness at the bottom of a carbon steel pipe for different superficial gas and liquid velocities in three-phase horizontal slug flow with 5 % water cut.

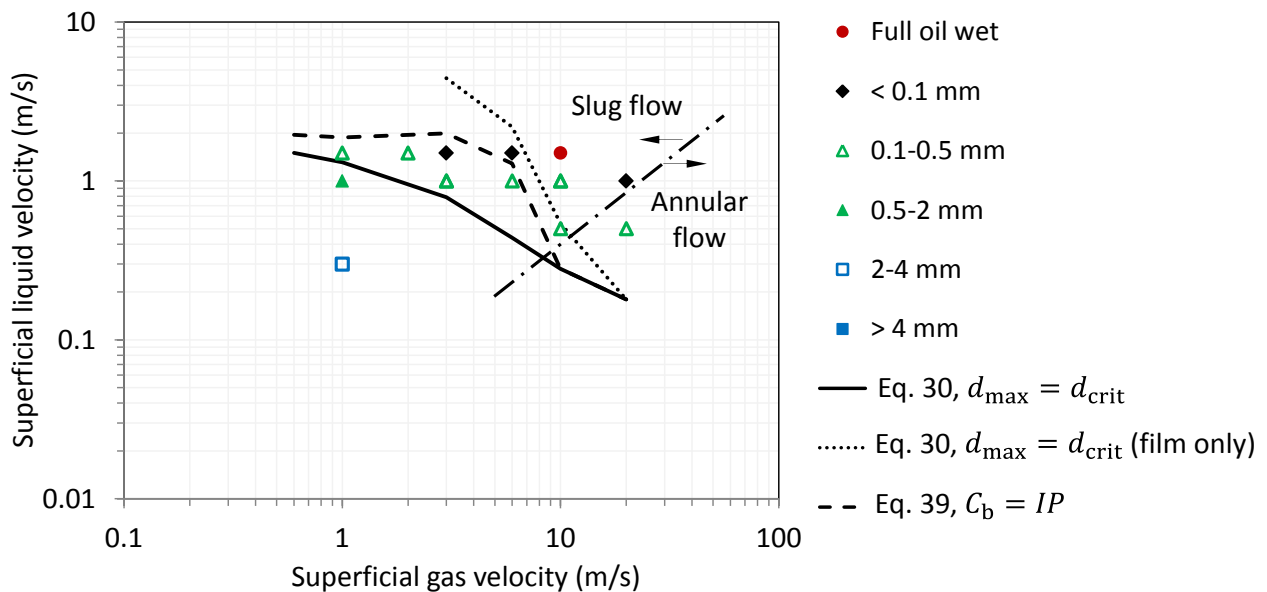


Figure 16: Modeled transition lines for dispersed liquid-liquid flow on experimental maps of phase wetting and water layer thickness at the bottom of a carbon steel pipe for different superficial gas and liquid velocities in three-phase horizontal slug flow with 10 % water cut.

It is known that the criteria provided by Brauner⁵ and developed in equation (30) do not fully represent the problem of dispersed liquid-liquid flow in pipes as discussed elsewhere,^{8, 33} since droplet concentration of the dispersed phase is unaccounted for. If water droplet concentration at the pipe bottom is large enough to reach a critical concentration where droplets are no longer stable and agglomerate; for example, a concentration similar to the phase inversion point (*IP*), the formation of water streams is inevitable. Unfortunately, the complex nature of slug flow makes the estimation of the concentration of dispersed droplets in the liquid very difficult since flow characteristics at a given pipe

section change intermittently. However, some approximation of the droplet concentration can be made by using the transport (advection-diffusion) equation and considering that droplet concentration only varies in time or the longitudinal direction of the pipe (x), and vertical direction (y , as indicated in Figure 13):

$$\frac{\partial C}{\partial t} - \varepsilon \frac{\partial^2 C}{\partial y^2} + u_{ds} \cos \beta \frac{\partial C}{\partial y} = 0 \quad (35)$$

where C is the water droplet concentration, t (s) is the time, ε is the droplet turbulent diffusivity (m^2/s), and u_{ds} (m/s) is the settling velocity of water droplets. No slip between water and oil phases is considered; thus, water droplets are considered to follow instantaneously the oil flow in the pipe direction (y), maintaining the volumetric water content (ε_w) constant. The advection of droplets in the y direction due to cross flow components in the liquid slug cylinder is neglected.

Mean droplet size represented as the Sauter mean diameter (d_{32}) can be used to characterize the behavior of the entire water droplet population. Experimental work on droplet sizes in horizontal oil-water pipe flow showed that the mean droplet size ranges from 0.38 to 0.45 of the maximum droplet size.^{34,35} In this case, the mean droplet size is approximated as:

$$d_{32} = 0.4 d_{\max} \quad (36)$$

Then the settling velocity of the mean droplet is calculated as:

$$u_{ds} = \left[\frac{3 d_{32} (\rho_w - \rho_o) g}{4 \rho_o C_D} \right]^{1/2} \quad (37)$$

where the droplet drag coefficient (C_D) is calculated using equation (25) with the droplet Reynolds number as in equation (26) but using u_{ds} as the droplet velocity and d_{32} as the droplet size.

The droplet turbulent diffusivity ε is considered to vary as a function of time as:

$$\begin{aligned} \varepsilon(t) &= \zeta \frac{D_{lf}}{2} \sqrt{\frac{\tau_{lf}}{\rho_o}}; & f_s^{-1}(i-1) < t \leq f_s^{-1}(1-\beta_s) i & \quad i = 1, 2, \dots, n \\ \varepsilon(t) &= \zeta \frac{D}{2} \sqrt{\frac{\tau_{ls}}{\rho_o}}; & t > f_s^{-1}(1-\beta_s) i & \quad i = 1, 2, \dots, n \end{aligned} \quad (38)$$

where ζ is the dimensionless eddy diffusivity that is considered constant with a value 0.255, as suggested by Karabelas.³⁶

Equation (34) is then solved numerically using a constant liquid height (h , m, see Figure 13) calculated from the average liquid holdup in the slug unit (α_1). This is a coarse approximation used to facilitate droplet mass continuity requirement at the transition from the liquid film to the slug cylinder. Forces on droplets, related to the hydrodynamic boundary layer (e.g., Saffman), are not considered. The water mass is assumed to remain constant across the pipe cross-section ($\int C(y) dA = \varepsilon_w A \alpha_1$), the net flux of droplets at the pipe walls and at the top of the liquid layer is zero ($u_{ds} \cos \beta C - \varepsilon \frac{\partial C}{\partial y} = 0$).

Figure 17 shows an example of water droplet concentration at the pipe bottom (C_b) as a function of time calculated with equation (35) for three-phase flow with superficial liquid velocity of 1 m/s, superficial gas velocity of 3 m/s and 5 % water cut. The water droplet concentration at pipe bottom remains similar to the average volumetric water content (5 %) when the liquid slug cylinder passes indicating homogeneous dispersion at the pipe cross-section. Nevertheless, the water droplet concentration increases reaching values as high as 48 % for the liquid film flow. It is worth reminding that at this specific flow condition, the criteria in equation (30) ($d_{\max} \leq d_{\text{crit}}$, solid line in Figure 15) predicts full dispersion of water droplets. However, unstable water wet and water layers of average thickness from 0.1 mm to 0.5 mm were measured at the pipe bottom (see Figures 11 and 15). This is unsurprising given the results from equation (35), since the phase inversion point (IP) of the oil-water system used in the experiments was measured to be about 25 % referred to the water content (Table 1). Accumulation of water droplets in concentrations similar or above the IP (as seen in Figure 17) can lead to

agglomeration and coalescence phenomena at the pipe bottom and, consequently, the formation of water streams and the occurrence of water wetting.

Therefore, to avoid agglomeration and coalescence of water droplets it is suggested to keep the water droplet concentration at the pipe bottom below a value not larger than the phase inversion point:

$$C_b \leq IP \quad (39)$$

Transition lines calculated using the criterion in equation (39) are shown in Figures 14, 15 and 16 as dashed lines. It can be seen that for 1 % water cut, the transition line from the criterion $C_b \leq IP$ is similar to the transition line obtained with the criteria $d_{max} \leq d_{crit}$. However, for the larger water cuts (5 % and 10 %) criterion $C_b \leq IP$ represents better the experimental behavior, predicting reasonably well the higher superficial liquid velocities needed to obtain full liquid-liquid dispersion; and thus, oil wet regime. Some under prediction of the critical superficial liquid velocity is found for superficial gas velocities of about 6 m/s or above. This would be related to the fact that slug flow is close to transition to annular regime as indicated by the experimental dash-dot line in Figures 14, 15 and 16 and, thus, liquid slugs may be less intense and relatively shorter than estimated by the simplified gas-liquid model introduced above.

An advantageous feature of the transport model in equation (35) is that it can describe how uniformly water droplets are dispersed across the liquid cross-section as a function of time depending on the slug frequency and the relative slug length. Therefore, in cases where the flow of the liquid slug may lead to full entrainment, it is possible to determine if dispersion is maintained in the liquid film or not.

In the case of annular or stratified gas-liquid flow patterns, a simple two-layer gas-liquid model can be used to obtain the liquid flow characteristics needed to assess the criteria via equations (30) and (39).

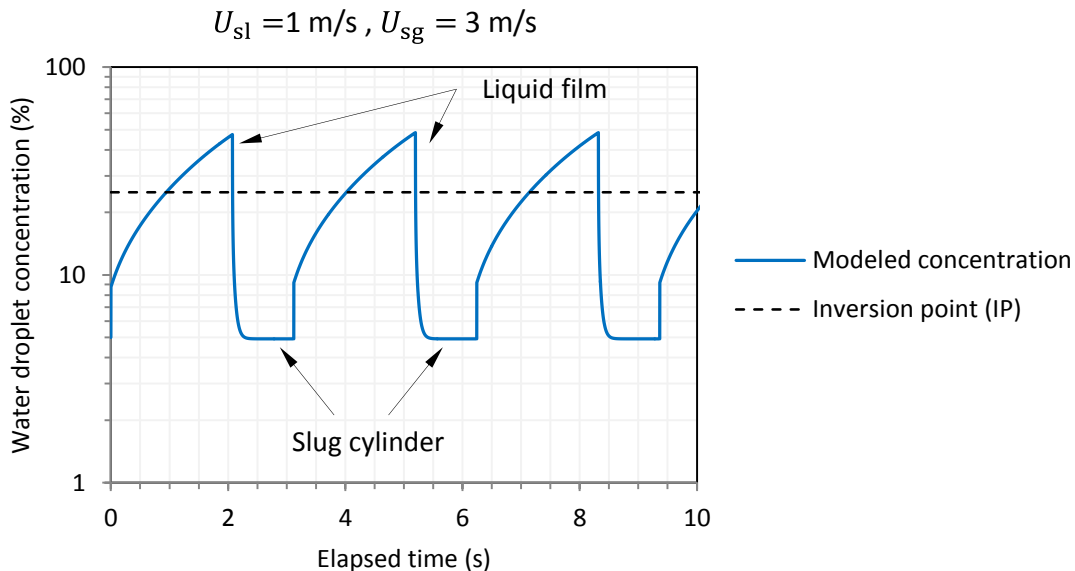


Figure 17: Example of water droplet concentration at the pipe bottom (C_b) in function of time calculated for three-phase horizontal slug flow with 5 % water cut.

General modeling considerations

From the hydrodynamic modeling approaches analyzed above, it is clear that predicting full liquid-liquid dispersion accurately in three-phase slug flow requires, at least, the combination of a gas-liquid model and specific criteria evaluated for the liquid mixture flow as outlined by Bonizzi et al.¹⁷ With regards to the latter, the criteria provided by Brauner⁵ (equation (30)) seems to be useful to predict the onset of full liquid-liquid dispersion, and so water wet to oil wet transition when the flow characteristics of the liquid mixture are averaged from both the liquid film and the slug cylinder. This approach shows good agreement with experimental data for 1 % water cut, but underpredicts the water wet to oil wet

transition for larger water cuts (5 % and 10 %). This would be related to the fact that accumulation of water droplets at the pipe bottom is unanticipated and, for relatively large water cuts, this can lead to excessively large concentrations where droplets are prone to agglomerate and coalesce forming water streams and causing water wetting.

More sophisticated methods, such as the implementation of a transport model (equation (35)) where water droplet concentration can be estimated as a function of time for the liquid film and the slug cylinder flow, are shown to be promising when used in combination with the criterion that water droplet concentration at the pipe bottom must be kept lower than the phase inversion point (equation (39)). Transition lines calculated with this approach agree well with all the available experimental data.

In practice, the use of the simplest criteria in equation (30) (and also equation (34)), which only involve droplet deposition risk, may lead to good enough approximation of the liquid-liquid dispersion bound in three-phase slug flow. This is due to the fact that, in general, the phase inversion of crude oil and water mixtures occurs at relatively high water contents (for example, 50 %); thus, the risk of water droplet agglomeration and coalescence at the pipe bottom may be less important than droplet deposition.

Recommendations for corrosion risk assessment

Currently, best practices of pipeline integrity management use Internal Corrosion Direct Assessment (ICDA) methods. A crucial part of these evaluations is to predict if a corrosive water phase effectively wets the internal pipe wall. In general, simple rules of thumb are used to determine water wetting; for example, liquid velocities below 1 m/s and water cuts above 20 %. However, it has been demonstrated in this work that the presence of a gas phase and slug flow pattern can lead to water wetting, even in flow conditions where water cut is relatively low (< 10 %) and superficial liquid and gas velocities are relatively high (> 1 m/s). Therefore, it is highly recommended to incorporate the use of hydrodynamic models, such as the ones introduced above, to predict water wetting in ICDA practices. Due to their mechanistic nature, these models can produce outputs for a wide range of fluid properties (e.g., oil, water and gas densities and viscosities, and oil-water interfacial tension) and oil, water and gas flow rates, with more confidence than other methods.

CONCLUSIONS

- Phase wetting regime and water layer thickness were successfully characterized in a carbon steel pipe of 0.1 m ID in three-phase oil-water-gas horizontal flow by using HF impedance probes located around the pipe circumference.
- Water wetting in horizontal slug flow is predominant at the pipe bottom (6 o'clock position) where thicker segregated water layers are detected. These layers would be formed by deposition, with agglomeration and coalescence of sinking water droplets.
- The thickness of water layers developed at the pipe bottom can vary significantly with time. Water preferably segregates at the liquid film region and then is partially or totally swept off and entrained by the passage of the liquid slugs. These effects lead to either intermittent water wet or intermittent oil wet regimes.
- Very thin water films (< 0.1 mm average thickness) are detected at the top and side pipe walls, especially for the largest tested water cut of 10 %. The formation of these films would be related to sporadic deposition of dispersed water droplets that rapidly come in contact with the pipe wall when slugs are developed.
- Oil wet regime can be achieved at the pipe bottom by increasing both superficial liquid and gas velocities. However, the first plays a more important role.
- Water layers detected at the pipe bottom become thicker for lower superficial liquid and gas velocities.

- Larger superficial liquid and gas velocities are required to fully disperse the water phase at the pipe bottom when water cut increases.
- A mechanistic model to assess full liquid-liquid (water-in-oil) dispersion in slug flow is introduced. It is based on the assumption that the liquid mixture is already dispersed, and specific stability criteria (e.g., droplet deposition and droplet accumulation at the pipe bottom) are evaluated relating to the liquid mixture flow. A steady state gas-liquid slug flow model is first used to estimate the characteristics of the liquid mixture flow at the film and the slug cylinder regions.
- The proposed model shows good agreement with the available experimental data, particularly when droplet accumulation at the pipe bottom is assessed.
- Since the prediction of water wetting is a crucial part of ICDA methods, it is highly recommended to incorporate mechanistic models such as those introduced in this work, which represent an upgrade to outdated rules of thumb.

ACKNOWLEDGEMENTS

The author acknowledges BP, ConocoPhillips, Enbridge, ExxonMobil, Petronas, Total and Shell for their financial support. Invaluable contribution of Mr. Lucas Idacir Sbrugnera Nazato as well as assistance from laboratory engineers and technicians at the Institute of Corrosion and Multiphase Technology is also greatly appreciated.

REFERENCES

1. M.B. Kermani, A. Morshed, "Carbon Dioxide Corrosion in Oil and Gas Production - A Compendium," *Corrosion* 59, 8 (2003): p 659.
2. S.N. Smith, M.W. Joosten, "Corrosion of Carbon Steel by H₂S in CO₂ Containing Oilfield Environments," CORROSION/2006, paper no. 6115 (Houston, TX: NACE, 2006), p. 26.
3. G. Aspenes, L.E. Dieker, Z.M. Aman, S. Høiland, A.K. Sum, C.A. Koh, E.D. Sloan, "Adhesion force between cyclopentane hydrates and solid surface materials," *Journal of Colloid and Interface Science* 343, 2 (2010): p 529.
4. U. Lotz, L.v. Bodegom, C. Ouwehand, "The Effect of Type of Oil or Gas Condensate on Carbonic Acid Corrosion," *Corrosion* 47, 8 (1991): p 636.
5. N. Brauner, "The prediction of dispersed flows boundaries in liquid-liquid and gas-liquid systems," *International Journal of Multiphase Flow* 27, 5 (2001): p 885.
6. A. Segev, "Mechanistic Model for Estimating Water Dispersion in Crude Oil Flow," Annual AIChE Meeting, paper no. 124a (San Francisco, CA: AIChE, 1984), p. 37.
7. J.L. Trallero, *Oil-Water Flow Patterns in Horizontal Pipes*, PhD thesis (Tulsa, OK: University of Tulsa, 1995).
8. L.D. Paolinelli, S. Nestic, "Hydrodynamic and Phase Wetting Criteria to Assess Corrosion Risk in Two-Phase Oil-Water Pipe Flow," CORROSION/2016, paper no. 7408 (Houston TX: NACE International, 2016), p. 19.
9. M. Açıkgöz, F. França, R.T. Lahey, "An experimental study of three-phase flow regimes," *International Journal of Multiphase Flow* 18, 3 (1992): p 327.
10. L. Pan, *High pressure three-phase (gas/liquid/liquid) flow*, PhD thesis (London, UK: University of London, 1996).
11. C. Keskin, H.-Q. Zhang, C. Sarica, "Identification and Classification of New Three-Phase Gas/Oil/Water Flow Patterns," SPE Annual Technical Conference and Exhibition, paper no. 110221 (Anaheim CA: Society of Petroleum Engineers, 2007), p. 13.
12. G. Ersoy, C. Sarica, E. Al-Safran, H.-q. Zhang, "Experimental Investigation of Three-Phase Gas-Oil-Water Slug Flow Evolution in Hilly-Terrain Pipelines," SPE Annual Technical Conference and Exhibition, paper no. 146630 (Denver CO: Society of Petroleum Engineers, 2011), p. 23.
13. G. Ersoy, C. Sarica, E. Al-Safran, H.Q. Zhang, "Three-phase gas-oil-water flow in undulating pipeline," *Journal of Petroleum Science and Engineering* 156, (2017): p 468.

14. M.O. Er, *Onset to separated water-layer in three-phase stratified flow*, MSc thesis (Tulsa OK: The University of Tulsa, 2010).
15. K.E. Kee, M. Babic, S. Richter, L. Paolinelli, W. Li, S. Nestic, "Flow Patterns and Water Wetting in Gas-Oil-Water Three-phase Flow – A Flow Loop Study," CORROSION/2015, paper no. 6113 (Houston, TX: NACE, 2015), p. 16.
16. L.D. Paolinelli, J. Yao, A. Rashedi, "Phase wetting detection and water layer thickness characterization in two-phase oil-water flow using high frequency impedance measurements," *Journal of Petroleum Science and Engineering* 157, (2017): p 671.
17. M. Bonizzi, R.I. Issa, "On the simulation of three-phase slug flow in nearly horizontal pipes using the multi-fluid model," *International Journal of Multiphase Flow* 29, 11 (2003): p 1719.
18. Y. Taitel, A.E. Dukler, "A model for predicting flow regime transitions in horizontal and near horizontal gas-liquid flow," *AIChE Journal* 22, 1 (1976): p 47.
19. D. Barnea, "A unified model for predicting flow-pattern transitions for the whole range of pipe inclinations," *International Journal of Multiphase Flow* 13, 1 (1987): p 1.
20. D.G.K. Aboud, A.-M. Kietzig, "Splashing Threshold of Oblique Droplet Impacts on Surfaces of Various Wettability," *Langmuir* 31, 36 (2015): p 10100.
21. F. Ayello, W. Robbins, S. Richter, S. Nestic, "Model Compound Study of the Mitigative Effect of Crude Oil on Pipeline Corrosion," *Corrosion* 69, 3 (2013): p 286.
22. S. Richter, M. Babic, X. Tang, W. Robbins, S. Nestic, "Categorization of Crude Oils Based on Their Ability to Inhibit Corrosion and Alter the Steel Wettability," CORROSION/2014, paper no. 4247 (Houston, TX: NACE, 2014), p. 16.
23. K.E. Kee, *A Study of Flow Patterns and Surface Wetting in Gas-Oil-Water Flow*, PhD thesis (Athens, OH: Ohio University, 2014).
24. A.E. Dukler, M.G. Hubbard, "A Model for Gas-Liquid Slug Flow in Horizontal and Near Horizontal Tubes," *Industrial & Engineering Chemistry Fundamentals* 14, 4 (1975): p 337.
25. K.H. Bendiksen, D. Maines, R. Moe, S. Nuland, "The Dynamic Two-Fluid Model OLGA: Theory and Application," *SPE Production Engineering* 6, 2 (1991): p 171.
26. G.A. Gregory, M.K. Nicholson, K. Aziz, "Correlation of the liquid volume fraction in the slug for horizontal gas-liquid slug flow," *International Journal of Multiphase Flow* 4, 1 (1978): p 33.
27. G.A. Gregory, D.S. Scott, "Correlation of liquid slug velocity and frequency in horizontal cocurrent gas-liquid slug flow," *AIChE Journal* 15, 6 (1969): p 933.
28. H.C. Brinkman, "The Viscosity of Concentrated Suspensions and Solutions," *The Journal of Chemical Physics* 20, (1952): p 571.
29. M. Wegener, N. Paul, M. Kraume, "Fluid dynamics and mass transfer at single droplets in liquid/liquid systems," *International Journal of Heat and Mass Transfer* 71, (2014): p 475.
30. J.O. Hinze, "Fundamentals of the hydrodynamic mechanism of splitting in dispersion processes," *AIChE Journal* 1, 3 (1955): p 289.
31. Y. Mlynek, W. Resnick, "Drop sizes in an agitated liquid-liquid system," *AIChE Journal* 18, 1 (1972): p 122.
32. J.T. Davies, "Calculation of critical velocities to maintain solids in suspension in horizontal pipes," *Chemical Engineering Science* 42, 7 (1987): p 1667.
33. B.F.M. Pots, J.F. Hollenberg, E.L.J.A. Hendriksen, "What are the Real Influences of Flow on Corrosion?," CORROSION/2006, paper no. 6591 (Houston, TX: NACE, 2006), p. 17.
34. P. Angeli, G.F. Hewitt, "Drop size distributions in horizontal oil-water dispersed flows," *Chemical Engineering Science* 55, 16 (2000): p 3133.
35. A.J. Karabelas, "Droplet size spectra generated in turbulent pipe flow of dilute liquid/liquid dispersions," *AIChE Journal* 24, 2 (1978): p 170.
36. A.J. Karabelas, "Vertical distribution of dilute suspensions in turbulent pipe flow," *AIChE Journal* 23, 4 (1977): p 426.